



ANALYSIS RE-ENTRANT HONEYCOMB AUXETIC STRUCTURE FOR LUMBAR VERTEBRAE USING FINITE ELEMENT ANALYSIS

Ai'man A'siqin Zulkefli¹, Muhammad Hazli Mazlan¹, Hiromitsu Takano², Abdul Halim Abdullah³,
 Muhammad Hilmi Jalil⁴ and Mohammad Azeeb Mazlan⁵

¹Department of Electrical and Electronic Engineering, Universiti Tun Hussien Onn Malaysia, Parit Raja, Johor, Malaysia

²Department of Orthopedic Surgery, Juntendo University, Tokyo, Japan

³School of Mechanical Engineering, College of Engineering, Universiti Teknologi MARA, Shah Alam, Malaysia

⁴Faculty of Mechanical and Automotive Engineering Technology, Universiti Malaysia Pahang, Pekan, Pahang, Malaysia

⁵AA3D Technology Sdn Bhd, Shah Alam, Selangor, Malaysia

E-Mail: mhazli@uthm.edu.my

ABSTRACT

Lumbar spinal fusion is a frequent surgical solution among people who are experiencing severe persistent lower back pain. One treatment option is Lateral Lumbar Interbody Fusion (LLIF) surgery. In the medical field, finite element analysis (FEA) can be used to predict the best surgical plan. LLIF surgery involves implanting an interbody cage into the disc space, which may potentially move to regain the disk height while helping stabilize the vertebral bones. In this study, FEA was applied using Mechanical Finder software (MF) to develop a 3D spine model lumbar vertebrae of the fourth and fifth lumbar vertebrae (L4 - L5) with the interbody cage design. The cage was made of polyether ether ketone (PEEK) and designed using Solidworks software. Given the auxetic structure's outstanding energy absorption capabilities, a re-entrant auxetic structure core with a novel sandwich panel was implanted between the lumbar vertebrae L4 and L5, as determined by CT scans using MF software. The model was analyzed in MF to assess the strength and fracture risk analysis of the interbody cage, with the results compared to mechanical properties values obtained by applying compression load (1000 N) to simulate spinal movements. Stress and strain distribution rates were exhibited when applying a force of 1000 N. The findings underscore the relevance of cage design, namely the surface endplate, in mitigating undesirable occurrences associated with cage sinking. To attain enough strength under typical conditions, a lumbar cage with a re-entrant auxetic construction has been proposed.

Keywords: finite element analysis, re-entrant auxetic structure, sandwich panel, fracture risks.

Manuscript Received 25 March 2024; Revised 28 May 2024; Published 7 July 2024

INTRODUCTION

Vertebral fusion is a surgical procedure used to deal with abnormalities of the spinal discs among people suffering from severe persistent lower back pain. The ongoing effects of disc disease might cause numbness, weakness, discomfort in the legs or arms, and low-level chronic pain (Battié *et al.*, 2019; Gupta *et al.*, 2016; Rossedeutsch *et al.*, 2017). Spinal fusion is a surgical procedure that joins two or more vertebrae to form an individual solid bone by introducing an intervertebral body fusion cage into the disc. The basic goal of spinal fusion is to reconstruct disc height, reduce uncomfortable movement, and increase the spine's stability. The disc comprises the inner nucleus pulposus, primarily made up of water and collagen, serving as shock absorbers. Surrounding it, the outer annulus fibrosus provides a flexible barrier between the vertebrae (Nizam *et al.*, 2021). As individuals age, the amount of water in their spinal discs diminishes, leading to reduced flexibility. Consequently, the discs shrink, and the spaces between the vertebrae narrow.

Lumbar Lateral Interbody Fusion (LLIF) is a surgical procedure to relieve back pain that involves removing a damaged disc and replacing it with an interbody cage or bone graft (Abhijit Y. Pawar *et al.*, 2015). This surgery is a less intrusive technique for interbody fusion that focuses on the waist's side (Abhijit

Pawar *et al.*, 2015; Stephan N. Salzmann *et al.*, 2017). This approach is traditionally performed on the left or right side, particularly for the second lumbar spine vertebrae (L2) through the fifth lumbar spine vertebrae (L5), due to the greater delicacy of the vena cava compared to the aorta, and the more lateral position of the right iliac vein in comparison to the left. LLIF also avoids exposing larger vessels, decreases blood loss, and reduces postoperative pain (Kirnaz *et al.*, 2020; Ralph J. Mobbs *et al.*, 2015). LLIF access enables expansion of the surface area, implant size, and bone graft, facilitating the aggressive restoration of disc height (Ralph J. Mobbs *et al.*, 2015; Stephan N. Salzmann *et al.*, 2017). Studies have demonstrated that LLIF is highly effective in preserving disc height using a wider interbody cage. Mechanical testing has shown LLIF to provide greater stability and superior resistance to subsidence compared to other techniques (Agarwal *et al.*, 2020; Peck *et al.*, 2018; Stephan N. Salzmann *et al.*, 2017). The Posterior Lumbar Interbody Fusion (PLIF) cage, on the other hand, has been shown to influence stress behavior and strength. Additionally, PLIF may pose challenges in correcting the coronal imbalance, restoring lordosis, and preparing the endplates (Abhijit Y. Pawar *et al.*, 2015; Ralph J. Mobbs *et al.*, 2015).

The cage's subsidence risk is caused by a combination of factors, including the cage structure



(shape, porosity, endplate) and the implant material. The cage design has a significant impact on the vertebral bones when implanted. Polyether ether ketone (PEEK) is extensively employed as a cage material, which offers stability and reduces the stress on the vertebral endplates (Campbell *et al.*, 2020). The elasticity modulus of PEEK material closely approaches that of bone; it has radiolucent qualities in imaging and biocompatibility, and the modulus of elasticity is comparable to that of cortical bone (Liao *et al.*, 2008). The implanted cage has an impact due to the stress behavior and the strength. It can lead to the failure to let the bone grow and lead to the adjacent level disorder. The cage might move from its correct position between two levels of vertebral bone after implantation. It can lead to the failure to let the bone grow and lead the cage to move from its position (Mazlan *et al.*, 2017). The revision surgery was needed to correct the location of the cage. Stress shielding occurs when implants take the load instead of the bone, and the bone loses density because of implant insertion to repair the fracture. Force transmission promotes osteoporosis, decreasing stress shielding and promoting osteoporosis in neighboring bones over time.

Auxetic structures and materials having a negative Poisson's ratio (down to -1) are of interest because of their peculiar behavior in deformation response, energy absorption qualities, and long-term durability. All auxetic cellular substances are design-driven, and their properties may be altered by modifying the unit cell arrangement. Several designs for two-dimensional (2D) and three-dimensional (3D) auxetic cellular structures have arisen in the recent decade, including re-entrant, chiral, lozenge, square grid, rotating rectangle, and triangular forms (Yang *et al.*, 2015). Auxetic materials have been considered for numerous medical purposes from the initial study in this subject since some biological tissues behave similarly. Auxetic metamaterials are a promising candidate for interaction with the human body owing to their lightweight construction and biocompatible design (Lvov, Senatov, Korsunsky, *et al.*, 2020; Lvov *et al.*, 2023). Another potential use for auxetic structures is bodily protection from impact loads in the construction sector, sports, and warfare. Auxetic foams have been utilized as shock-absorbing sections of protective safety helmets, ensuring that when the material is pushed in one direction, it expands in others, avoiding fracture and attempting to reduce the likelihood or seriousness of injury (Lvov, Senatov, Stepashkin, *et al.*, 2020). Auxetics, with their improved mechanical properties and Poisson's ratio, have potential in biomedical applications like orthopedic prostheses and bone implants. They resist long-term cyclic loads, making them a viable alternative to conventional load-bearing systems. However, limited study suggests a gap between 2D auxetic components (Lvov, Senatov, Korsunsky, *et al.*, 2020).

This research seeks to create a three-dimensional (3D) vertebral model using Computed Tomography (CT) scan pictures. Then, interbody cages with re-entrant honeycomb structure and surface roughness of endplates constructed of PEEK material will be created and tested

for strength using stress and strain distributions. Studies suggest auxetic structures can improve mechanical energy dissipation by absorbing less energy than non-auxetic structures, while sandwich panels are proposed as protective structures. The finite element approach was employed to evaluate the strength of the lumbar vertebrae and spinal cage, using PEEK as the cage's construction material, as it offers the advantage of replicating the real condition of the spinal structures after the implantation of the interbody cages under the designated loads. The finite element approach provides a way to analyze stress and strain with complete mechanical characteristics, repeatability, and high-level controllability (Zhang *et al.*, 2016). Sandwich panels with re-entrant honeycomb auxetic structural core may enhance the chances of successful operations, improve implant fit, and enhance force and load transmission.

METHODOLOGY OF 3D VERTEBRAL MODEL WITH INTERBODY FUSION CAGE

The Research Design of the Project

The study utilized MECHANICAL FINDER™ software to extract L4 and L5 vertebrae from CT scan images and DICOM files, a medical imaging format, as Figure-1 depicts the flowchart of the study. An interbody cage was created using Solidworks 2022 software. The implant was virtually inserted between the L4 and L5 vertebrae in Mechanical Finder software for finite element analysis (FEA). The model underwent a compression load of 1000 N to replicate real-world spinal movements. The models were exposed to steadily increasing compressive loads ranging from 1 k to 10 kN, with continuous processes used to establish failure probabilities and yielding element distributions. 'Dale' Bass *et al.* used ten iterations to simulate traumatic loading conditions, with a 50% injury risk expected at a maximum load of 10 kN ('Dale' Bass *et al.*, 2008; Mazlan, 2016). The FEA focused on evaluating the strength of the designed interbody cage and the surrounding vertebral bones. This numerical analysis was performed using Mechanical Finder software.

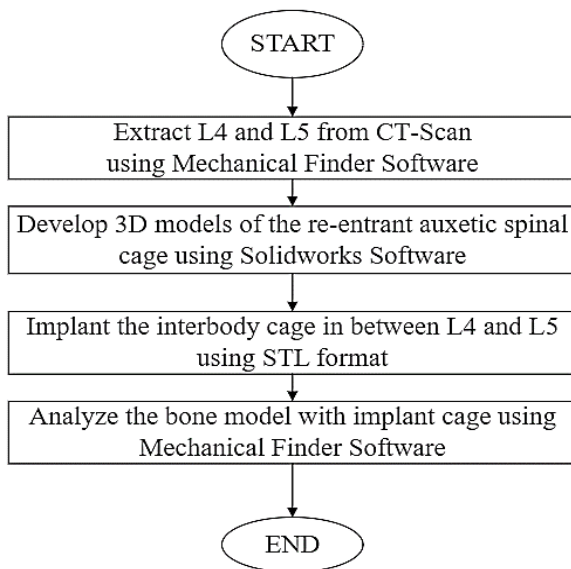


Figure-1. Flowchart of the study.

Vertebral Bone Model

The 3D vertebral bone model of L4-L5 vertebrae was created using CT scan image data and Mechanical Finder software from the Research Center of Computational Mechanics Co. Ltd. Japan. The anatomical structures were generated by delineating cortical bone outer boundaries, allowing visualization, and using tetrahedral components to simulate the vertebral bone's even surface (Takano *et al.*, 2017). The vertebral bodies are characterized by a cancellous bone core encased in a 0.4 mm cortical shell, with intervertebral discs, cancellous bone, and facet joint cartilages represented using 1.0 mm solid tetrahedral elements and cortical bone using 1.0 mm linear shell triangular elements. The model consists of 84,856 tetrahedral solid elements and 13,770 triangular shell elements, as shown in Figure-2.

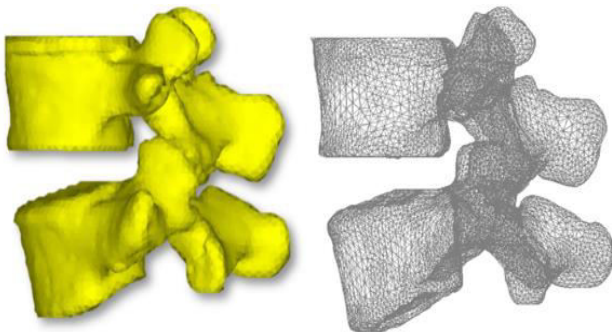


Figure-2. Vertebral bone model of L4 and L5.

Interbody Cage Development

The dimension of the 3D interbody cage was designed to be 26 mm in length, 16 mm in height, and 10 mm in width using the Solidworks software, according to the requirements needed to withstand load on the spinal segments following implantation. The 3D model was created by adjusting the interbody cage and merging the

geometries of the auxetic metamaterial and honeycomb structure using the solid-state modeling approach with the SOLIDWORKS © 2022 software. In this research, there are two types of interbody fusion cage implants were designed, namely re-entrant honeycomb auxetic structure and modified auxetic structure implant cage. The modified auxetic structure implant cage was added with a unique sandwich panel design with a re-entrant honeycomb auxetic structure as shown in Figure-3. The implants were saved in stereolithography (STL) format then exported to Mechanical Finder software and inserted into the intervertebral gap to mimic the real environment of the LLIF for simulation purposes.

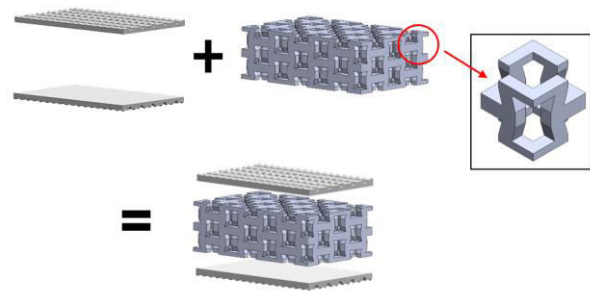


Figure-3 (a). A novel sandwich panel with a re-entrant honeycomb structure core.

Figure-3 and Figure-4 show the isometric views of the interbody cages (RH auxetic structure and modified auxetic structure, respectively). The implants were then exported to Mechanical Finder software and implanted into the vertebral bone model for FEA purposes.

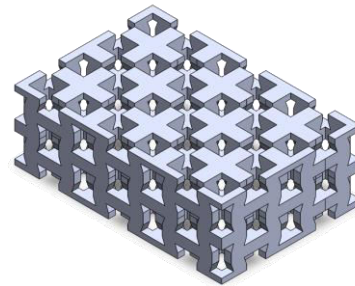


Figure-3 (b). The isometric view of the RH auxetic structure interbody cage.

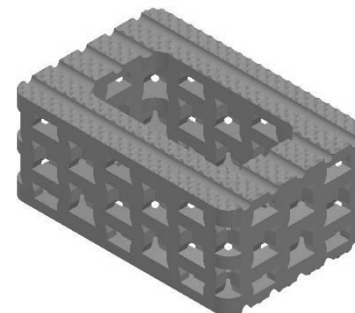


Figure-4. The isometric view of the modified auxetic structure interbody cage.

Implantation of the Interbody Cage in Between the L4 and L5



The interbody cage was virtually implanted in the Mechanical Finder and positioned between L4 and L5, as shown in Figure-5.

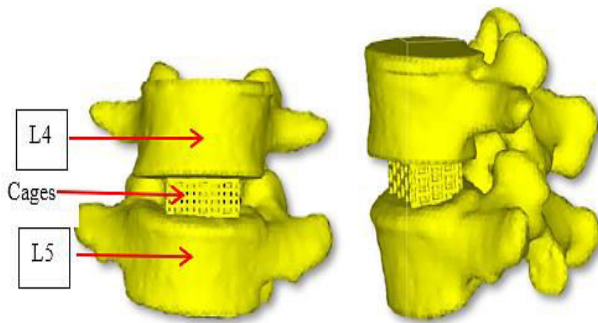


Figure-5. The implantation of the interbody cage into the L4 and L5 spine segments.

Material Properties

The material properties for the vertebral and interbody cages are shown in Table-1 and Table-2. The top of L4 was applied with compression loads ranging from 1 to 10 kN, and the lowermost part of L5 was constrained in all directions, as shown in Figure-6.

Table-1. Mechanical properties of PEEK (Jalil *et al.*, 2017)

Material	Mechanical parameter	Value	Unit
PEEK	Young's Modulus	3620	MPa
	Density	1320	$\frac{Kg}{cm^2}$
	Poisson ratio	0.39	-
	Yield Stress	98	MPa
	Ultimate Tensile strength	100	MPa

Table-2. Material Properties of Bone (Mazlan *et al.*, 2020)

Young's Modulus E (MPa)	Bone density $\rho(g/cm^3)$
$E = 0.01$	$\rho = 0.0$
$E = 33,900\rho^{2.20}$	$0.0 < \rho \leq 0.27$
$E = 5,307\rho + 469$	$0.27 < \rho < 0.6$
$E = 10,200\rho^{2.01}$	$0.6 < \rho$
Yield stress	Bone density $\rho(g/cm^3)$
$\alpha = 1.0 \times 10^{20}$	$\rho \leq 0.2$
$\alpha = 137\rho^{1.88}$	$0.2 < \rho \leq 0.317$
$\alpha = 114\rho^{1.72}$	$0.317 \leq \rho$
Poisson's ratio	Bone density $\rho(g/cm^3)$

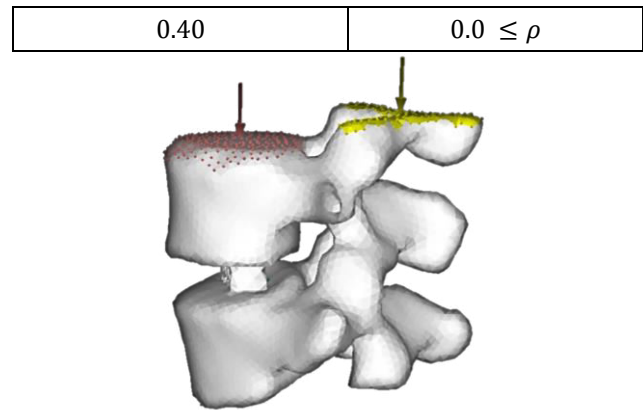


Figure-6. Load applied on top of fourth lumbar.

RESULTS AND DISCUSSIONS

The maximum principal and equivalent stress were used to analyze the strength of the interbody cage. The equal stress was utilized to identify if the material would fail or yield under the applied loads. In contrast, the maximum principal stress was used to evaluate material failure when the maximum principal stress exceeded the ultimate tensile strength. The evaluation was performed based on the compression load applied to recreate the spine's physiological motion. The results were used to assess the biocompatibility and strength of the structure.

Equivalent Stress on the Interbody Cage and Vertebral Bone Model

According to the results in Table-3 and Table-4, the RH auxetic structure resulted in a higher equivalent stress on the vertebral bone (25.11 MPa) and on the cage itself (85.18 MPa) compared to the modified auxetic structure implant cage. In contrast, the modified auxetic structure implant cage produced higher equivalent stress on the bone (9.40 MPa) and on the cage (71.69 MPa). The modified auxetic structure interbody cage produced the lowest stresses on the bone and the cage construct for the normal and the worst-case scenarios. The stress values produced by both cages were likewise lower than the yield strength of bone and cage for this configuration under typical load circumstances. The modified auxetic structure generates the highest difference value between yield stress and the produced equivalent stress for bone and cage compared to the RH auxetic structure. This criterion is very important since it will reflect the low possibility of bone and cage failures. The results show that the lower the value maximal equivalent stress of the implant cage, the stronger the cage, stress shielding is reduced and the risk of cage to failure is also lower. The 10kN compressive load was utilized to replicate the most severe situation, which is the force that poses a 50% chance of damage. The highest range of equivalent stress of interbody cage stress during compression motion was set at 98 MPa (the value of yield strength) when the pressure of the load is 10 kN (in the worst-case scenario) to see which cage designs can withstand the pressure.

However, the equivalent stresses generated on the cages are comparably higher and significantly surpass the



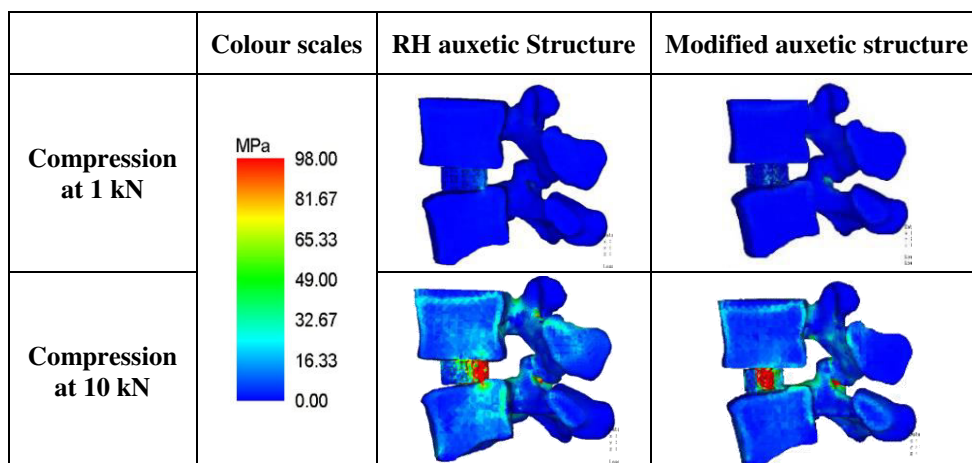
yield strength of the cage material. These results show that all the cage constructs are at risk of cage failure under the worst-case load scenario. Under the worst loading conditions, the RH auxetic structure resulted in a higher equivalent stress on the vertebral bone (1646.14 MPa) and on the cage itself (2761.77 MPa) compared to the modified auxetic structure implant cage. In contrast, the modified auxetic structure implant cage produced higher equivalent stress on the bone (1013.75 MPa) and on the cage (1672.04 MPa). The percentage difference in yield strength and equivalent stress of the cage for the modified auxetic structure is 26.84% while for the RH auxetic structure is 13.08%. According to Abdullah and Zulkefli *et*

al. (Abdullah, 2021; Zulkefli *et al.*, 2024), the interbody cage with a 70% infill density is deemed the most efficient design because it produces the lowest value of equivalent stress. Consequently, the likelihood of bone failure for the modified auxetic structure interbody cage is very low compared to other cage setups (Mazlan *et al.*, 2020; Rho *et al.*, 1998). As indicated by the small percentage difference between yield strength and equivalent stress, the interbody cage's structural integrity deteriorates, increasing the cage's danger. This indicates that the implanted modified auxetic structure interbody cage has the highest structural ability compared to the RH auxetic structure core only.

Table-3. Maximal equivalent stress of bone and cage implant as compared to their associated yield strength (Load at normal condition, 1k N, and load at the worst-case scenario, 10 kN).

Physiological Motion	Interbody Cage	Yield Strength of bone (MPa)	Equivalent Stress of bone (MPa)	Yield Strength of PEEK Material (MPa)	Equivalent Stress of cage implant (MPa)
Compression at 1 kN	RH auxetic Structure	83	25.11	98	85.18
	Modified auxetic structure	83	9.40	98	71.69
Compression at 10 kN	RH auxetic Structure	83	1646.14	98	2761.77
	Modified auxetic structure	83	1013.75	98	1672.04

Table-4. Equivalent stress results under compression loads when the maximum range of equivalent stress is set at 98 MPa.



Maximum Principal Stress on the Interbody Cage and Vertebral Bone Model

The integrity of the cage and the bone was evaluated by comparing the maximum principal stress and

the ultimate tensile strength of the cage and the bone. The cage structure and bone undergo failure when the maximum principal stress surpasses the ultimate tensile strength. Table-5 summarizes the maximum principal



stress for those conditions. The compression motion for normal conditions resulted in maximum principal stress for bone and cage in the RH auxetic structure (21.39 MPa and 40.25 MPa, respectively) compared to the modified auxetic structure implant cage (8.42 MPa and 48.41 MPa respectively). For the worst-case condition, the compression motion resulted in maximum principal stress for bone and cage in the RH auxetic structure (1130.61 MPa and 1513.32 MPa, respectively) compared to the modified auxetic structure implant cage (1003.79 MPa and 1783.75 MPa respectively). Table-6 shows the maximum principal stress distribution on the vertebral bones under normal and worst-case conditions. The results show that the maximum principal stress is far below the maximum principal stress for the cage constructs and the bones. This indicates that the chances of cage and bone failures can be

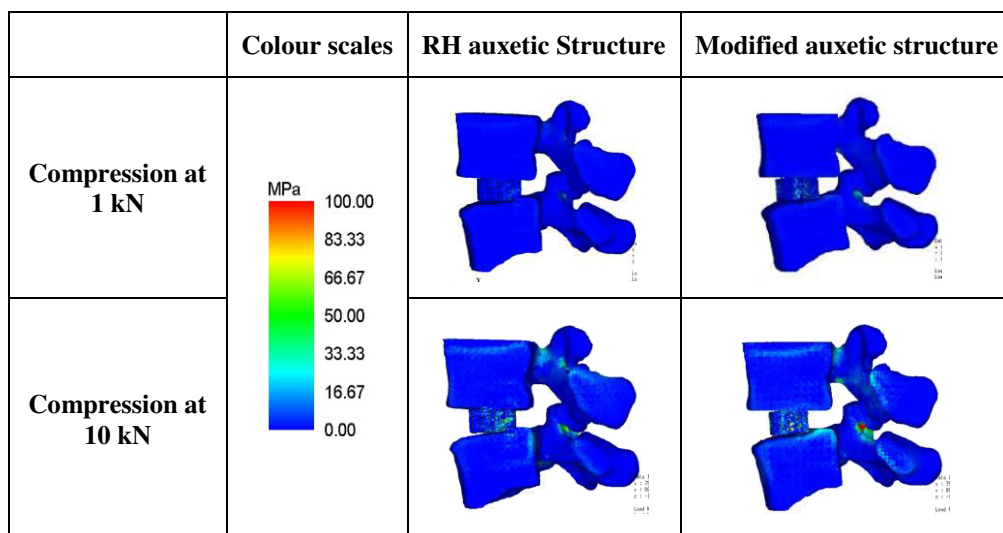
significantly avoided. The results also show that the modified auxetic structure has the lowest maximum principal stress for the normal and worst-case settings. A higher infill density resulted in higher impact strength, such as the modified auxetic structure (Qamar Tanveer *et al.*, 2022). Therefore, as the percentage difference decreases, the interbody cage structure becomes weaker, increasing the risk of failure.

These results demonstrate that this honeycomb infill pattern, with the specified infill densities, exhibits the best structural integrity, minimal impact on the bones compared to other patterns, and the ability to sustain static loads applied to cage structures. The study found that modified auxetic structures often outperformed RH auxetic structures in terms of stiffness, compressive strength, and shear.

Table-6. Maximal maximum principal stress of bone and cage implant as compared to their associated ultimate tensile strength (Load at normal condition, 1k N and load at worst-case scenario, 10 kN).

Physiological Motion	Interbody Cage	Ultimate Tensile Strength of bone (MPa)	Maximum Principal Stress of bone (MPa)	Ultimate Tensile Strength of cage (MPa)	Maximum Principal Stress of cage (MPa)
Compression at 1 kN	RH auxetic Structure	130	21.39	100	40.25
	Modified auxetic structure	130	8.42	100	48.41
Compression at 10 kN	RH auxetic Structure	130	1130.61	100	1513.32
	Modified auxetic structure	130	1003.79	100	1783.75

Table-7. Maximal maximum principal stress under compression loads when the maximum range of equivalent stress was set at 100 MPa.





Failure Element Analysis

Figure-7 shows the average equivalent stress of the vertebral bones. The models were exposed to steadily increasing compressive loads ranging from 1 k to 10 kN, with continuous processes used to establish failure probabilities and yielding element distributions. Ten iterations were used to recreate traumatic loading conditions, with the vertebral body's ultimate compressive strength of 8000 N. The maximum load that is expected to create a 50% risk of injury is 10 kN according to 'Dale' Bass *et al.* ('Dale' Bass *et al.*, 2008; Mazlan, 2016). The total number of failure and yielding elements under gradually increasing load for the RH auxetic structure was 0, 5, 1 659, 5 087, 5 965, 6 593, 7 283, 8 380, 9 787 and 11 154 elements, while for the modified auxetic structure was 0, 0, 22, 836, 4 929, 5 888, 6 513, 7 439, 9 317 and 10 386 elements, respectively. The RH auxetic interbody cage model showed an abrupt change in the number of the deformation elements after achieving its onset fracture load (5 elements), which was 2 kN. In contrast, for the modified implant cage, the number of the deformation elements increased gradually after their corresponding onset fracture loads were initiated at 3 kN, respectively which is 22 elements. This graph shows the same trend from 1 to 10 kN which is RH auxetic structure greater number of elements than modified auxetic structures. Thus, the modified auxetic structure interbody cage was shown to be the optimum therapeutic method since the danger of cage sinking is minimized.

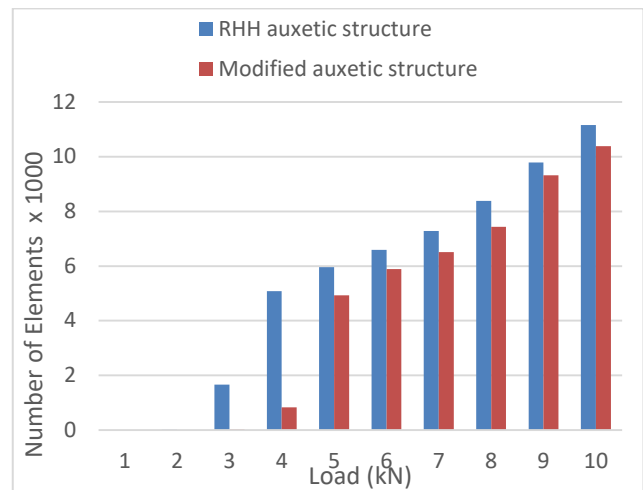


Figure-7. Changes of failure element distributions of interbody cages.

A graphical illustration of failure element distributions using 10 kN as a 50% risk of injury is presented in Table 7. The green dots reflect tensile strength, the yellow points signify compressive yielding, and the red patches represent compressive failure. The findings indicate that the modified auxetic structure implant cage construct (10386 elements) had the fewest number of distorted parts when compared to the RH implant cage model (11154 elements).

RH auxetic Structure			
	Number of failure elements: 11154		
Modified auxetic structure			
	Number of failure elements: 10386		
	Side View	Inferior surface of L4	Superior surface of L5

The results show that the re-entrant auxetic structure core with a new sandwich panel is the most efficient (Y. Chen & Wang, 2022; Wang *et al.*, 2018). This is due to it having demonstrated the highest structural capability in comparison to the other cage designs. The outcomes show that when the material's yield and ultimate tensile strength exceed the equivalent and maximum principal stress, the probability of cage failure is reduced.

Furthermore, the stress was predicted to be distributed mainly on the lateral part of the implant, reducing the possibility of cage subsidence into the vertebral endplate, especially near the cage edge (Jalil *et al.*, 2017; Mazlan *et al.*, 2020).

According to the findings, even under the worst possible circumstances, the modified auxetic structure implant cage has created the lowest equivalent stress



during the physiological spine motions. These results indicate that the modified auxetic structure implant cage has the highest structural ability compared to other interbody cages. Higher equivalent stress might significantly increase the probability of bone and cage failures. The data show that employing this material might greatly reduce stress shielding and improve load sharing. These results were evidenced by the lower stress levels generated by auxetic structures with microporous/rough surface endplate constructs. The results show that the lower the value between maximum principal stress and ultimate tensile strength, the weaker the interbody cage construct and the higher the risk of cage failure.

The modified auxetic structure fabricated from PEEK material with the surface roughness of the endplate is recommended for implantation in spinal bones. This preference stems from the observation that PEEK cages exhibit lower stress levels and reduced subsidence effects when constructed with higher infill density. Moreover, augmenting layer thickness enhances impact strength while diminishing tensile strength. Notably, an FEA conducted by Chen *et al.* (Z. Chen *et al.*, 2023) underscores the efficacy of surface modification (surface pattern), demonstrating significantly lower rates of cage failure compared to alternative infill patterns in vertebral bone models and promoting better osteogenic activity and osseointegration. The paramount criteria for characterizing cage biocompatibility in LLIF surgery, as highlighted by previous research (Mazlan *et al.*, 2020) emphasize low stiffness followed by high yield and ultimate tensile strength. Nizam *et al.* (Nizam *et al.*, 2021) further corroborate these findings, indicating that PEEK cages possess superior structural integrity due to their ability to generate lower stress levels compared to cages made of alternative materials. Consequently, it is imperative to consider that PEEK-based cages with higher infill density exhibit relatively lower stress production than those with lesser infill density.

CONCLUSIONS

In conclusion, this study has effectively achieved its objectives. The rigidity and strength of a 3D structure are impacted by its infill pattern. Results revealed that the modified auxetic structure is better compared to the RH auxetic structure interbody cages. Increased infill density enhances the material's tensile and compressive strength. Additionally, the roughness of the endplates lowered the cage and block stiffness. Lower infill density creates air space between each layer (Z. Chen *et al.*, 2023), leading to variations in the component's strength. The modified auxetic structure showed the lowest maximum principal and equivalent stresses, making it the strongest in terms of structural capabilities compare to the auxetic structure without surface roughness (Z. Chen *et al.*, 2023; Fernandez-Vicente *et al.*, 2016; Wang *et al.*, 2018). The lower generation of maximum principal and equivalent stresses in comparison to yield strength and ultimate tensile strength of the material of the cage can significantly reduce the risk of the cage and bone failures. The successful evaluation of this surface modification

method on intervertebral fusion cages demonstrated its promise for future clinical use. The results show that both the porous design characteristics of the stress-optimized body lattice and the microporous endplates significantly reduced cage stiffness. Recommendations for future work include (i) conducting 3D prints using a more durable metallic material such as PEEK-rGO, (ii) 2. The computational models have been enhanced by considering the reactions of major spinal muscles, tendons, and ligaments, and (iii) performing material nonlinear analysis to handle better fracture, plasticity, and crushing or cracking elements.

ACKNOWLEDGEMENTS

We express our sincere appreciation to our colleagues at Juntendo University, Japan, whose valuable insights and expertise significantly contributed to this research. This research was supported by Universiti Tun Hussein Onn Malaysia which provides monetary assistance through (vot Q287).

REFERENCES

- Abdullah, N. S. 2021. Design and Simulation Study of Posterior Lumbar Interbody Fusiom (PLIF) Cage for Three-Dimensional (3D) Printing Application. Universiti Tun Hussein Onn Malaysia.
- Abhijit P., Alexander H., Federico G., Andrew S., Darren L., and Frank C. 2015. Lateral Lumbar Interbody Fusion—Outcomes and Complications _ Enhanced Reader. *ASIAN SPINE JOURNAL*, 9(6): 978–983.
- Abhijit Y. P., Alexander P. H., Andrew A. S., Federico P. G., Darren R. L., and Frank P. C. 2015. A Comparison study of LLIF and PLIF in Degenerative Lumbar Spondylolisthesis. *Asian Spine Journal*, 668–674.
- Agarwal, N., White, M. D., Zhang, X., Alan, N., Ozpinar, A., Salvetti, D. J., Tempel, Z. J., Okonkwo, D. O., Kanter, A. S., and Hamilton, D. K. 2020. Impact of endplate-implant area mismatch on rates and grades of subsidence following stand-alone lateral lumbar interbody fusion: An analysis of 623 levels. *Journal of Neurosurgery: Spine*, 33(1): 12–16.
- Battié, M. C., Joshi, A. B., and Gibbons, L. E. 2019. Degenerative Disc Disease: What is in a Name? *Spine*, 44(21) : 1523–1529.
- Campbell, P. G., Cavanaugh, D. A., Nunley, P., Utter, P. A., Kerr, E., Wadhwa, R., and Stone, M. 2020. PEEK versus titanium cages in lateral lumbar interbody fusion: A comparative analysis of subsidence. *Neurosurgical Focus*, 49(3).
- Chen, Y., and Wang, Z. W. 2022. In-plane elasticity of the re-entrant auxetic hexagonal honeycomb with hollow-circle joint. *Aerospace Science and Technology*, 123.



Chen, Z., Chen, Y., Wang, Y., Deng, J. J., Wang, X., Wang, Q., Liu, Y., Ding, J., and Yu, L. 2023. Polyetheretherketone implants with hierarchical porous structure for boosted osseointegration. *Biomaterials Research*, 27(1).

Bass D., Rafaels C. R., Salzar K. A., Carboni R. S., Kent M., Lloyd R. W., Lucas M. D., Meyerhoff S., Planchak K., Damon C. A., and Bass G. T. 2008. Thoracic and lumbar spinal impact tolerance. *Accident Analysis & Prevention*, 40(2) : 487–495.

Fernandez-V. M., Calle W., Ferrandiz S. and Conejero, A. 2016. Effect of Infill Parameters on Tensile Mechanical Behavior in Desktop 3D Printing. *3D Printing and Additive Manufacturing*, 3(3).

Gupta V. K., Attry S., Vashisth N., Gupta E., Marwah K., Bhargav S., and Bhargav S. 2016. Lumbar Degenerative Disc Disease: Clinical Presentation and Treatment Approaches. *IOSR Journal of Dental and Medical Sciences*, 15(08).

Jalil M. H., Mazlan M. H., and Todo M. 2017. Biomechanical Comparison of Polymeric Spinal Cages Using Ct Based Finite Element Method. *International Journal of Bioscience, Biochemistry and Bioinformatics*, 7(2):110–117.

Kirnaz S., Navarro-Ramirez R., Gu J., Wipplinger C., Hussain I., Adjei J., Kim E., Schmidt F. A., Wong T., Hernandez R. N., and Härtl R. 2020. Indirect Decompression Failure After Lateral Lumbar Interbody Fusion—Reported Failures and Predictive Factors: Systematic Review. *Global Spine Journal*, 10(2_suppl): 8S-16S.

Liao J. C., Niu C. C., Chen W. J., and Chen L. H. 2008. Polyetheretherketone (PEEK) cage filled with cancellous allograft in anterior cervical discectomy and fusion. *International Orthopaedics*, 32(5) : 643–648.

Lvov V. A., Senatov F. S., Korsunsky A. M., & Salimon A. I. 2020. Design and mechanical properties of 3D-printed auxetic honeycomb structure. *Materials Today Communications*, 24.

Lvov V. A., Senatov F. S., Shinkaryov A. S., Chernyshikhin S. V., Gromov A. A., and Sheremetyer V. A. 2023. Experimental 3D printed re-entrant auxetic and honeycomb spinal cages based on Ti-6Al-4 V: Computer-Aided design concept and mechanical characterization. *Composite Structures*, 310.

Lvov V. A., Senatov F. S., Stepashkin A. A., Veveris A. A., Pavlov M. D., and Komissarov A. A. 2020. Low-cycle fatigue behavior of 3D-printed metallic auxetic structure. *Materials Today: Proceedings*, 33(4) :1979–1983.

Mazlan M. H. 2016. Biomechanical analysis of osteoporotic spines with diseases using CT-based finite element method. Kyushu University.

Mazlan M. H., Todo M., Ahmad I. L., Takano H., Yonezawa I., Abdullah A. H., Jalil M. H., and Nordin N. D. D. 2020. Biomechanical evaluation of two different types of interbody cages in posterior lumbar interbody fusion. *International Journal of Emerging Trends in Engineering Research*, 8(1 1.2 Special Issue): 221–226.

Mazlan M. H., Todo M., Yonezawa I., and Takano H. 2017. Biomechanical alteration of stress and strain distribution associated with vertebral fracture. *Journal of Mechanical Engineering*, SI 2(2): 123-133.

Nizam N. A. H. M., Mazlan M. H., Salleh N. S. M., Razali M. A., Abdullah A. H., Jalil M. H. A., Takano H., and Nordin N. D. D. 2021. Design and analysis of interbody fusion cage materials based on finite element analysis. 1st National Biomedical Engineering Conference, NBEC 2021, 7–12.

Peck J. H., Kavlock K. D., Showalter B. L., Ferrell B. M., Peck D. G., and Dmitriev A. E. 2018. Mechanical performance of lumbar intervertebral body fusion devices: An analysis of data submitted to the Food and Drug Administration. *Journal of Biomechanics*, 78: 87–93.

Qamar T. M., Mishra G., Mishra S., and Sharma R. 2022. Effect of infill pattern and infill density on mechanical behaviour of FDM 3D printed Parts- a current review. *Materials Today: Proceedings*, 62(1) : 100-108.

Ralph J. M., Kevin P., Grey M., Kevin S., and Prashanth J. R. 2015. Lumbar Interbody Fusion: Techniques, indications and comparison of interbody fusion options including PLIF, TLIF, MI-TLIF, OLIF/ATP,LLIF and ALIF. *Journal of Spine Surgery (Hong Kong)*, 1(1): 2–18.

Rho J. Y., Kuhn-Spearing L., and Zioupon P. 1998. Mechanical properties and the hierarchical structure of bone. *Medical Engineering and Physics*, 20(2): 92-102

Rosdeutsch A., Copley P., and Khan S. 2017. Degenerative spinal disc disease and its treatment. *Orthopaedics and Trauma*, 31(6): 378–387.

Stephan N. S., Jennifer S., and Alexander P. H. 2017. Lateral Lumbar Interbody Fusion—Outcomes and Complications _ Enhanced Reader. *Current Reviews in Musculoskeletal Medicine*. 10 (4): 539–546.

Takano H., Yonezawa I., Todo M., Mazlan H. M., Sato T., and Kaneko K. 2017. Biomechanical Study of Vertebral Compression Fracture Using Finite Element Analysis. *Journal of Applied Mathematics and Physics*, 05(04).

Wang Y., Zhao W., Zhou G., and Wang C. 2018. Analysis and parametric optimization of a novel sandwich panel



with double-V auxetic structure core under air blast loading. *International Journal of Mechanical Sciences*, 142–143, 245–254.

Yang L., Harrysson O., West H., and Cormier D. 2015. Mechanical properties of 3D re-entrant honeycomb auxetic structures realized via additive manufacturing. *International Journal of Solids and Structures*, 69–70. <https://doi.org/10.1016/j.ijsolstr.2015.05.005>

Zhang Z., Sun Y., Sun X., Li Y., Liao Z., and Liu W. 2016. Recent Advances in Finite Element Applications in Artificial Lumbar Disc Replacement. *Journal of Biomedical Science and Engineering*, 09(10): 1–8.

Zulkefli A. A., Mazlan M. H., Takano H., Salleh N. S. M., and Jalil M. H. 2024. Biomedical Analysis of Lateral Lumbar Interbody Fusion (LLIF) Cage for Lumbar Vertebrae. *Series on Biomechanics*. 38(1): 45-56.